Building a three-dimensional near-surface geologic and petrophysical model based on borehole data: A case study from Chémery, Paris Basin, France

Paola Sala, Marcel Frehner, Nicola Tisato, and O. Adrian Pfiffner

ABSTRACT

The fact that velocity models based on seismic reflection surveys commonly do not consider the near-surface geology necessitates filling the gap between the top of a velocity model and the surface of the Earth. In this study, we present a new workflow to build a shallow geologic model based exclusively on borehole data and corroborated by laboratory measurements. The study area is in Chémery (France), located at the southwestern border of the Paris Basin, where a large amount of borehole data is publicly available. The workflow starts with identifying lithologic interfaces in the boreholes and interpolating them between the boreholes. The three-dimensional (3-D) geometry of the lithologies then allows interpretation of the position, orientation, and offset of fault planes. Given the importance of the fault interpretation in the modeling process, a combination of different approaches is used to obtain the most reasonable structural framework. After creating a 3-D grid, the resulting 3-D structural model is populated with upscaled velocity logs from the boreholes, yielding the final near-surface P-wave velocity model. To better constrain the velocity model, we conducted laboratory measurements of P- and S-wave velocities in dry and water-saturated conditions on all lithologies in the model. The laboratory data were used to populate the 3-D near-surface model with V_P/V_S ratio values. The presented workflow accounts for one-dimensional borehole data and is much more iterative and time-consuming than

AUTHORS

PAOLA SALA ~ *Institute of Geological Sciences, University of Bern, Bern, Switzerland;* sala@geo.unibe.ch

Paola Sala is a Ph.D. student in the Tectonics Group of the University of Bern (Switzerland). After her M.Sc. degree in geology at the University of Milan (Italy), she worked as a software support geoscientist at Schlumberger. She went back to academia in 2010 focusing her research on three-dimensional geologic modeling techniques applied to various structural contexts (from intracratonic basins to fold-and-thrust belts).

MARCEL FREHNER ~ *Geological Institute, ETH Zurich, Zurich, Switzerland;* marcel.frehner@erdw.ethz.ch

Marcel Frehner obtained his Ph.D. in earth sciences from the ETH Zurich (Switzerland) and spent two years as a university assistant at the University of Vienna (Austria). Since 2011, he has been a research associate at the Geological Institute of ETH Zurich, coleading the Rock Physics Research Network. He specialized on numerical modeling and quantitative analysis of geologic and geophysical processes.

NICOLA TISATO ~ *Geological Institute, ETH Zurich, Zurich, Switzerland;* nicola.tisato@erdw.ethz.ch

Nicola Tisato is a Ph.D. student in the Structural Geology and Tectonics Group at the ETH Zurich (Switzerland). He obtained his M.Sc. degree in geology from the Università Degli Studi di Padova (Italy). His research focuses mostly on laboratory investigations of elasticity and seismic-wave propagation phenomena of fluid-saturated rocks at low seismic frequencies.

O. ADRIAN PFIFFNER ~ *Institute of Geological Sciences, University of Bern, Bern, Switzerland;* pfiffner@geo.unibe.ch

O. Adrian Pfiffner is emeritus professor at the Institute of Geological Sciences at the University of Bern (Switzerland), where he led the Tectonics Group. He attained a diploma in geology followed by a Ph.D. and a postdoctoral degree at the ETH Zurich (Switzerland). He then worked at the University of Neuchatel (Switzerland) before joining the University of Bern.

workflows based on two-dimensional seismic sections. Nevertheless, the workflow results in a robust 3-D near-surface model allowing for structural interpretations and revealing the 3-D seismic velocity field.

INTRODUCTION

Knowledge of the near-surface geology is fundamental for various engineering geologic applications, for exploration of resources, and for seismic acquisition and interpretation. For example, characterizing site-specific near-surface seismic amplification effects is essential for seismic hazard assessment, as demonstrated by Poggi et al. (2012) for the city of Lucerne and by Havenith et al. (2007) for the city of Basel (both in Switzerland), or for investigating the damage of past earthquakes (Fritsche and Fäh, 2009). Steiner et al. (2011) demonstrated that an accurate seismic velocity model for both P- and S-waves is essential for time-reverse imaging, which is a special type of full-waveform inversion applied to recordings of the ambient seismic wave field. Other important properties of the near-surface geology are, for example, porosity and permeability, which are necessary for accurate groundwater flow models or for identifying suitable deposit sites for hazardous waste.

Two-dimensional (2-D) or three-dimensional (3-D) seismic surveys routinely conducted by the exploration industry result in seismic sections or cubes that commonly do not include the top few tens or hundreds of meters below the surface of the Earth. Thereby, the seismic data are only processed below a certain predefined horizontal datum to avoid problematic issues with topography or near-surface low-velocity layers (Cox, 1999). Given the relevance of the near-surface geology, other methods have to be applied to fill the gap between the deeper seismic surveys and the surface of the Earth. Such near-surface models can be developed using a combination of different techniques. Possible near-surface seismic methods include uphole surveys, vertical seismic profile surveys, shallow reflection surveys, ground-penetrating radar, different inversion methods (e.g., surface-wave dispersion-curve inversion), refraction migration (traveltime or interferometric migration), and wave tomography (first-arrival traveltime or full-waveform tomography). An extensive overview of all of these methods is given by Miller et al. (2010). In addition, to better constrain the model, longitudinal and transversal seismic wave speeds can be measured for specimens collected in the field. Other nonseismic methods to investigate the near-surface geology include not only gravimetric and geoelectrical methods, but also traditional geologic field work,

the analysis of digital elevation models (DEM), or remote sensing. For example, Burtscher et al. (2012) were able to draw geologic conclusions solely based on the differential geometrical analysis of a DEM. However, a topography that mirrors relatively closely the underlying geology is necessary for a successful analysis of the DEM. Schober and Exner (2011) demonstrated how photogrammetry can be used to build a 3-D geologic model on the outcrop scale.

In this article, we demonstrate how to develop an integrated 3-D model of the shallow geology and of the shallow seismic velocity distribution using a large set of publicly available borehole data. The chosen study site is Chémery, a village between the regions of Touraine and Sologne in the southwestern part of the Paris Basin, France. In this area, an underground natural gas storage reservoir has been operated since the 1970s; therefore, the abundant easy accessibility of borehole data makes Chémery ideally suited to develop the methodology for 3-D modeling based on borehole data.

GEOLOGIC SETTING

The study area is located in the Sologne-Touraine region in the southwestern part of the Paris Basin, France (Figure 1), 5 km (3 mi) north of the village of Chémery. The Paris Basin is a nearly circular intracratonic sag basin, which started developing during a Permian-Triassic extensional tectonic phase. Its total sedimentary fill (Permian-Carboniferous through Holocene) reaches as much as approximately 3000 m (9843 ft) in thickness (Perrodon and Zabek, 1990). The basin trough lies above the Y-junction of three fault systems that separate the underlying basement into three major structural blocks. The study area is located in the eastern part of the Armorican block, which is the westernmost of the three major structural blocks of the Paris Basin. This block is bounded in the east by the north–northwest to south–southeast-striking Seine-Sennely fault network (Perrodon and Zabek, 1990; inset in Figure 1). North of the village Contres, the study area is limited by a major fault system perpendicular to the Sennely fault (Debeglia and Debrand-Passard, 1980).

Below the Chémery hill, which is the only topographic high, the study area (Figure 1) contains a natural gas storage reservoir operated for years by the company Gaz de France and, recently, by Storengy. The deepest boreholes in the storage site area reach the Permian strata, which do not outcrop here. The reservoirs are located at an average depth of approximately 1085 m (3560 ft) in Upper Triassic sandstones and Lower Jurassic shallow-marine limestones, both of which also cannot be studied in outcrops. A more extensive definition of the reservoir intervals and sedimentologic and stratigraphic reservoir characterization can be found in Grauls and Lafay (1979), Merzeraud (1992), Rauscher et al. (1992), Huault et al. (1995), Merzeraud et al. (1999), Merzeraud et al. (2000), Hamon and Merzeraud (2005).

Surface Geology

Outcrops in the study area (Figure 1) comprise Upper Cretaceous to Pliocene sedimentary rocks. The youngest deposits are fluvial terraces that cover most of the area east of the gas storage facility. Because of the very smooth topography and the intensive agricultural activity, outcrops are rare, and the most significant ones are in areas with restricted access (e.g., private caves and properties). Therefore, the previously compiled geologic map of the Contres-Romorantin area (Fleury, 1997) was drawn mainly with the help of borehole data and aerial photographs. Outcrops farther to the south of Chémery, close to the Cher River (Figure 1), contain well-exposed Cretaceous strata. A comparison of these strata with borehole information helped better interpret the regional geologic setting of the Chémery area.

Stratigraphy

The following brief description of the outcropping formations (Figure 2) provides details about lateral variation, repartition, composition, depositional environment, and thickness.

The Upper Cretaceous carbonate facies are generally proximal, with terrigenous components that are more frequent than in the rest of the Paris Basin
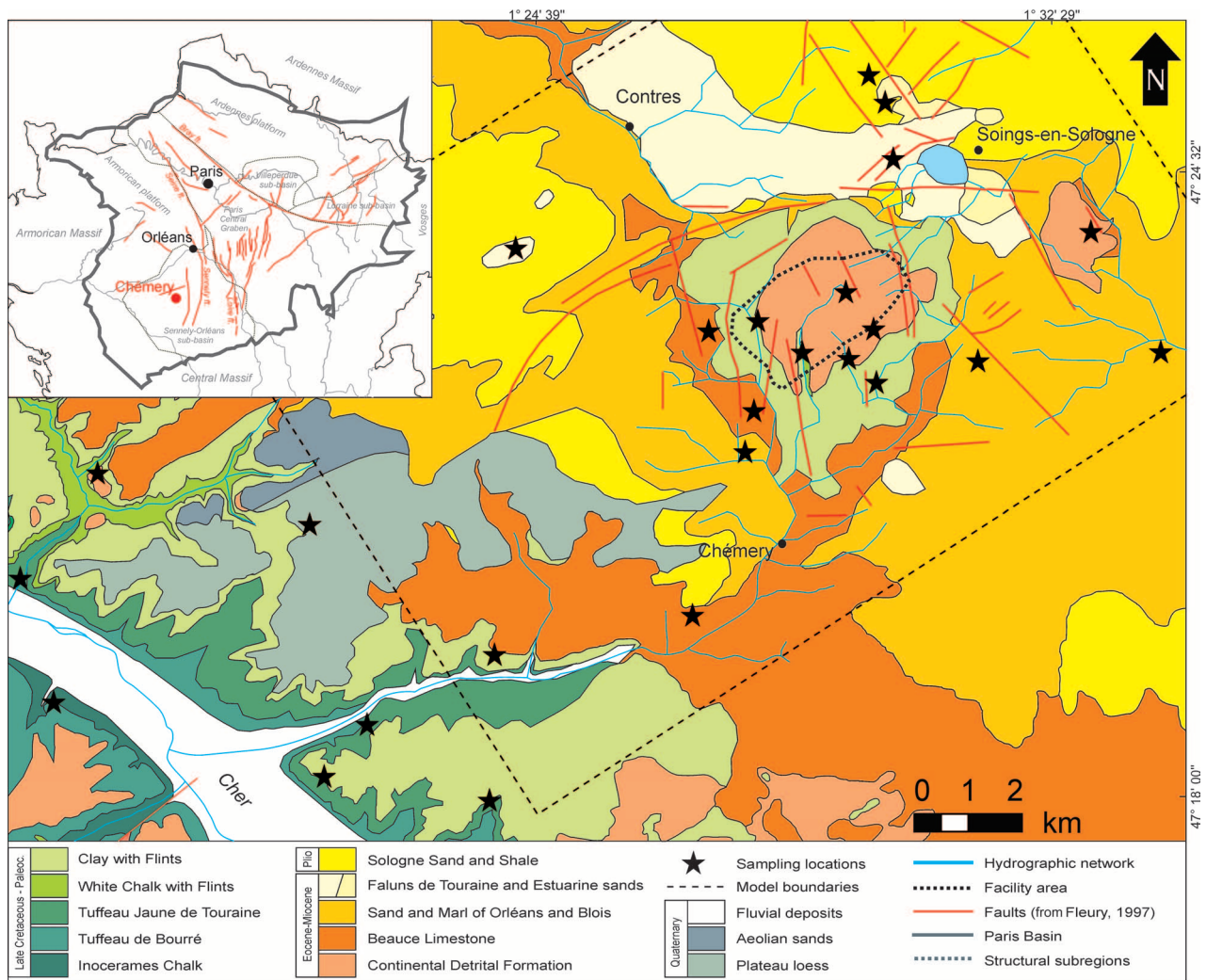
Figure 1. Geologic map of the study area in the Chémery region simplified from Fleury (1997). Colors represent the different lithologies according to Figure 2. The faults in red are from Fleury et al. (1997) in Upper Cretaceous strata at a depth of 30 to 150 m (98–492 ft). Only the fault in the Cher River bed is actually exposed at the surface. For a better visualization, some lithologies only locally outcropping are removed from the map (e.g., fluvial terraces east of the Chémery hill). The 25 sampling localities for laboratory testing are indicated as stars, but the sampled rocks do not necessarily correspond to the lithology shown on the map (e.g., when sampling occurred in caves). Inset shows the overview map of the Paris Basin (outlined as bold black line). The thin black line is the French border; thin gray lines are rivers; black dotted lines are approximate boundaries between the tectonic subregions of the Paris Basin; red lines are faults from Beccaletto et al. (2011). The coordinates are given in latitude and longitude.

(Robaszynski et al., 1982). The Turonian stage is represented by three main lithologies: the Inocerames Chalk at the base, which is a shaly chalk with black flints rich in bivalves; the middle Turonian Tuffeau Blanc (or Tuffeau de Bourré); and the upper Turonian Tuffeau Jaune de Touraine at the top. These formations are improperly called "chalk" because transmitted-light microscopy of thin sections reveals that the rocks have a mixed composition with detrital quartz grains (as much as 40%) and other minerals, such as mica and glauco-nite. These formations are characterized by a very high average porosity of 44% (Dessandier et al., 1996; Prigent, 1997).

The Turonian changes upward into a friable chalk with abundant gray flints. In the study area, the interval Coniacian–Campanian is represented by a sequence of laterally varying chalks, referred to as "White Chalk with Flints" (known in the French literature as "Craie Blanche à Silex"). The most representative strata are, from older to younger: the Villedieu Chalk, the Blois Chalk, and the Romorantin
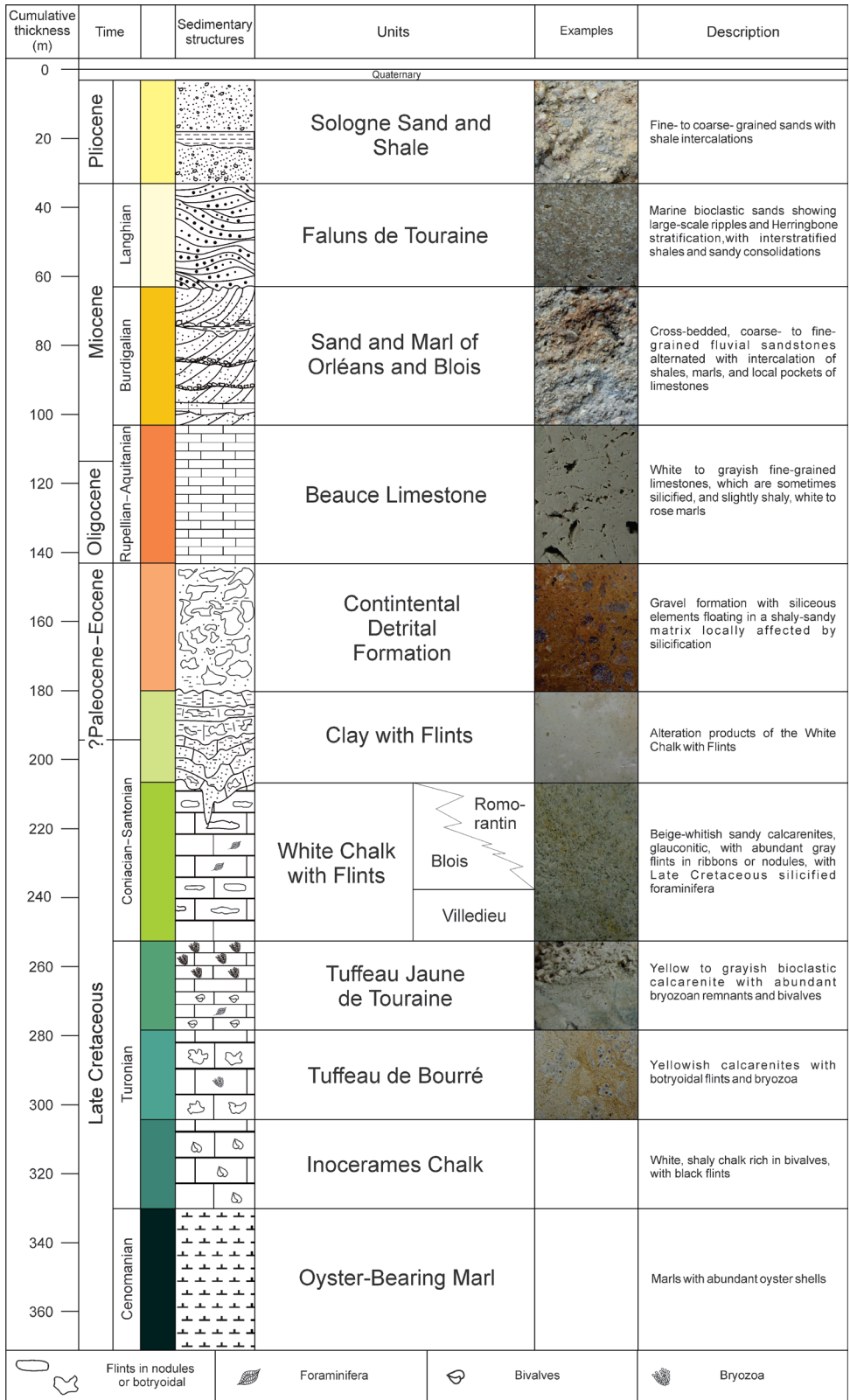
Figure 2. Stratigraphic column showing the lithologies outcropping in the study area. Colors are used throughout this article. The characteristic sedimentary features (bedding type, grain size, presence of chert) and fossil content (bivalves, foraminifera) of each specific formation are represented in symbolic form.

Chalk. The Villedieu Chalk constitutes an onlapping succession of calcarenites exhibiting several prominent laterally continuous hardgrounds and flint lines (Jarvis and Gale, 1984). The Blois Chalk is a pale-yellow calcarenitic chalk containing numerous closely spaced lines of light-gray to pink structured opal

cristobalite and tridymite–quartz sponge flints (Jarvis and Gale, 1984). Spicules of lithistid sponges are a major component of these flint-rich sediments, locally making up more than 75% of the rock. The spiculites are well-sorted packed biomicrites containing accessory (approximately 1%) pelletal glauconite. In the study area, the typical lithotype of the White Chalk with Flints is a beige-whitish chalk with flints; it is sandy, glauconitic, and rich in bryozoans. The thickness of this lithotype exceeds 46 m (151 ft) in the area (Fleury et al., 1997). During the Campanian, the chalk was exposed and underwent strong alteration (e.g., karst formation related to the dissolution of the carbonate), which led to the formation of the Clay with Flints (French: Argiles à Silex; Laignel et al., 1998). The thickness of this unit is extremely variable depending on the progression of the alteration front into the chalk. The average thickness is 26.5 m (86.9 ft) (Fleury et al., 1997).

The overlying Cenozoic formations start with the Continental Detrital Formation, a Paleocene–Eocene gravel formation that has siliceous elements floating in a shaly-sandy matrix locally affected by silicification. The thickness of this formation is strongly variable and reaches a maximum of 37 m (121 ft) (Fleury et al., 1997). In the model area (Figure 1), the formation appears to be restricted to the top of the Chémery hill and the neighboring Soings-en-Sologne structure, northeast of Chémery. Other outcrops are distributed along the Cher riverside.

The Eocene unit is followed by lacustrine limestones belonging to the Beauce Limestone (Ménillet and Edwards, 2000). This Aquitanian formation is formed by white to grayish fine-grained limestones, which are sometimes silicified, and slightly shaly, white to rose marls. The thickness ranges from some meters on the borders of the geologic map (Figure 1) to as much as 80 m (262 ft) close to Orléans (Fleury et al., 1997).

After the lacustrine episode represented by the Beauce Limestone, the fluvial deposits of the Sand and Marl of Orléans and Blois were deposited during the Burdigalian. This formation consists of an alternation of coarse sandstones, shales, marls, and, locally, limestones (Fleury et al., 1997).

The last marine ingression is represented by Langhian marine sandstones called "Faluns de Touraine," which locally show interstratified shales and sandy consolidations. The formation is limited to the north of the gas storage facility area and does not reach the Chémery hill. Its thickness can reach as much as 30 m (98 ft) (Fleury et al., 1997).

After the Miocene ingression, the sea retired completely, and fluvial sedimentation occurred again in the form of the Sologne Sand and Shale, which consists of heterometric quartzofeldsphatic sands with interstratified shales (Larue and Etienne, 1998, 2002). The thickness attains a maximum of 30 m (98 ft) (Fleury et al., 1997). Fleury (1997) described the presence of estuarine sandstones north of the gas storage facility, around the narrow marine inlet of Faluns de Touraine between the villages of Contres and Soings-en-Sologne.

Structural Geology

The Chémery hill is the surface expression of a buried dome structure, which is revealed in a north–south cross section (Fleury et al., 1997). In the map adapted from Fleury (Figure 1), the core is seen as undifferentiated Upper Cretaceous units capped by the Eocene detrital formation. Whereas the hill top lacks post-Eocene deposits, the latter surround the dome structure.

Several fault systems exist in the studied Chémery area, which affect a large part of the stratigraphic column down to Permian levels (Debeglia and Debrand-Passard, 1980). Based on thickness variations in interpreted seismic profiles, Debeglia and Debrand-Passard (1980) argue that some faults were already active in the Permian, Triassic, and Early Jurassic. One of the few outcropping faults affects Upper Cretaceous strata (southwest in Figure 1), which indicates that this fault was still active at that time. In the shallow boreholes, evidence of active faults can be found in even younger strata. This long-lasting fault activity suggests a reactivation of older faults until the Cenozoic.

To obtain further details about the structural and stratigraphic framework of the area, a set of cross sections were drawn across the Chémery area in the west–east and north–south direction (Figure 3),
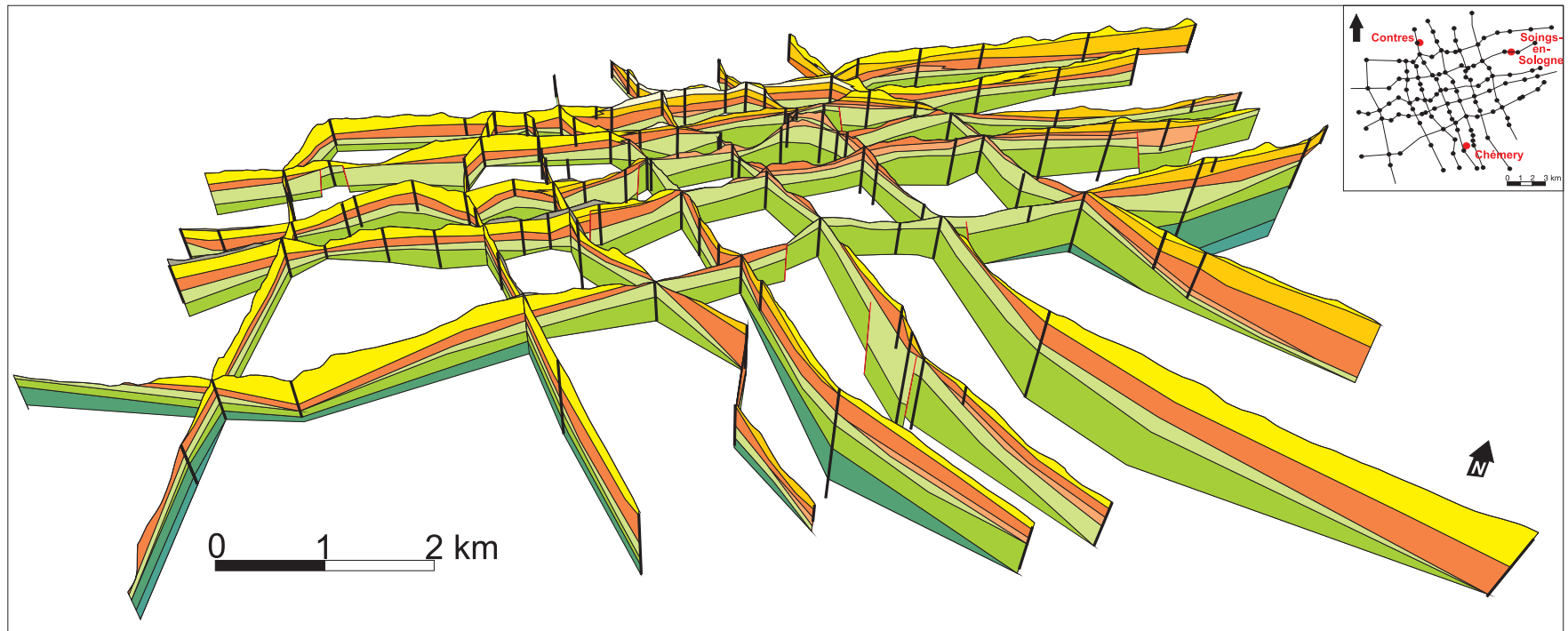
Figure 3. Exploratory fence diagram showing interpreted cross sections based on the lithologic information from shallow borehole data. Colors represent the different lithologies according to Figure 2. Black thick lines represent borehole traces.

considering altitude profiles obtained from the Shuttle Radar Topography Mission Digital Elevation Model (DEM) and a few borehole data from a public repository of the Bureau de Recherches Géologiques et Minières (BRGM; i.e., Geological Survey of France). The information inferred from the cross sections (Figure 3) is constructed from a small selected number of boreholes, whereas the well markers are interpolated linearly between the boreholes along the cross sections. This procedure leaves large gaps between the cross sections without any interpolated geologic information. Therefore, these cross sections alone provide a very limited amount of information. Nevertheless, a few of the main structural elements can be recognized, such as abrupt elevation changes of the lithologic interfaces, which can be indicative of faults. These faults cannot be mapped at the surface but may be correlated with a deeper fault system recognized in previously acquired seismic data (Fleury et al., 1997). Further details on the subsurface can only be provided by a 3-D geologic model to fill the gaps between the sections.

MODEL BUILDING

Basic Data

A total of 634 boreholes (Figure 4) plus topographic and geologic maps were considered as the base information for the generation of the 3-D geologic subsurface model. Thereby, the boreholes deliver one-dimensional (1-D) vertical data. This is distinctively different from the usual model building, for which 2-D seismic cross sections or 3-D seismic cubes are used as the base information. In this study, no such 2-D or 3-D information is used. Two groups of boreholes were available in this study (Figure 4): (1) 60 deep exploitation wells from Gaz de France with a depth of more than 1000 m (3281 ft) and (2) 574 shallow boreholes from BRGM with a depth of a few tens of meters. The deep boreholes are situated mainly around the Chémery hill. Some of them contain lithologic well markers from the surface down; others only contain lithologic well markers below the top of the Cenomanian Oyster-bearing

Marl. All borehole data are easily accessible via the BRGM geographic system Infoterre™ (BRGM, 2010). This repository contains data of thousands of wells across France. The data sheets may contain the borehole position, well path length, lithologic well markers, facies description, water table level, and other information. From the 574 shallow boreholes, approximately 150 contain uphole seismic surveys (i.e., velocity logs; Figure 4), which can be used to investigate, for example, low-velocity layers, the depth and velocity of the weathered near-surface layer, or the velocity of the deeper unweathered layers (Telford et al., 1990). From the seismic traveltime-depth relationships measured by the uphole surveys, it is possible to obtain a discrete velocity log for each borehole. The deep boreholes do not contain uphole seismic surveys because it was not possible to gather data from within the gas storage facility area.

The boundaries of the model and the sampling resolution are determined by the borehole data spacing. The horizontal extension of the model corresponds to a rectangle of 187 km^2 (72 mi^2) embracing the shallow wells and the extension of the underground natural gas reservoir (Figure 4). The top boundary of the model is the topography defined by the Shuttle Radar Topography Mission DEM. The geologic map (Fleury, 1997) traces the formation limits at the topographic surface, which allows for an accurate reconstruction of the lithologic interfaces close to the top of the model. The bottom boundary of the model is defined to be the top of the Oyster-bearing Marl (Figure 2). This boundary was chosen because the Cenomanian Oyster-bearing Marls are the shallowest marker that can be recognized in all the deep wells, allowing for connection between the shallow model and the deep strata. The base information was georeferenced and loaded into the Petrel E&P Software Platform (Schlumberger), which is also used for the entire 3-D modeling.

Stratigraphic Framework Modeling and Fault Detection

The usual workflow for model building based on seismic data starts with identifying faults in the
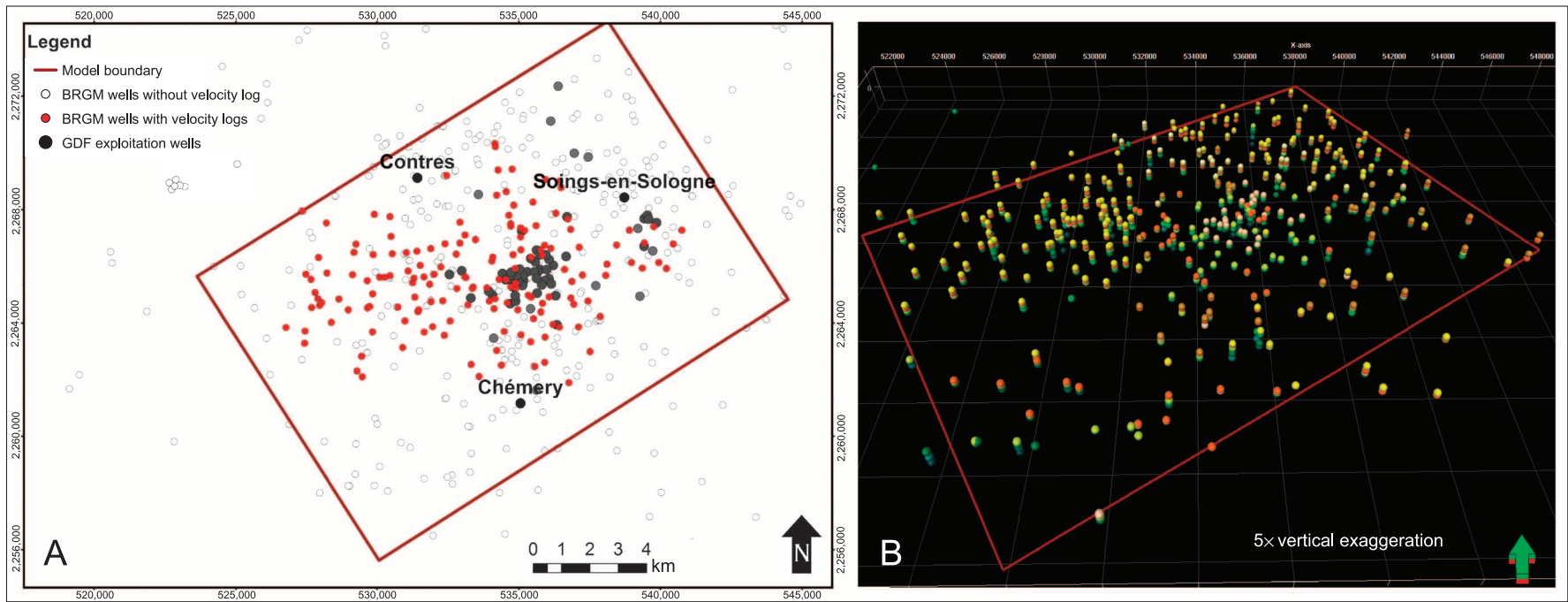
Figure 4. (A) Map view showing all available borehole data and the model boundary. Exploitation wells from Gaz De France (GDF) are commonly more than 1000 m (3281 ft) deep; Wells belonging to the database of the Bureau de Recherches Géologiques et Minières (BRGM) are commonly several tens of meters deep. (B) Oblique view of the lithologic well markers in the boreholes. The coordinates are given in the system NTF France II degrees.

Figure 5. Workflow for three-dimensional model building based on one-dimensional borehole data followed in this study.
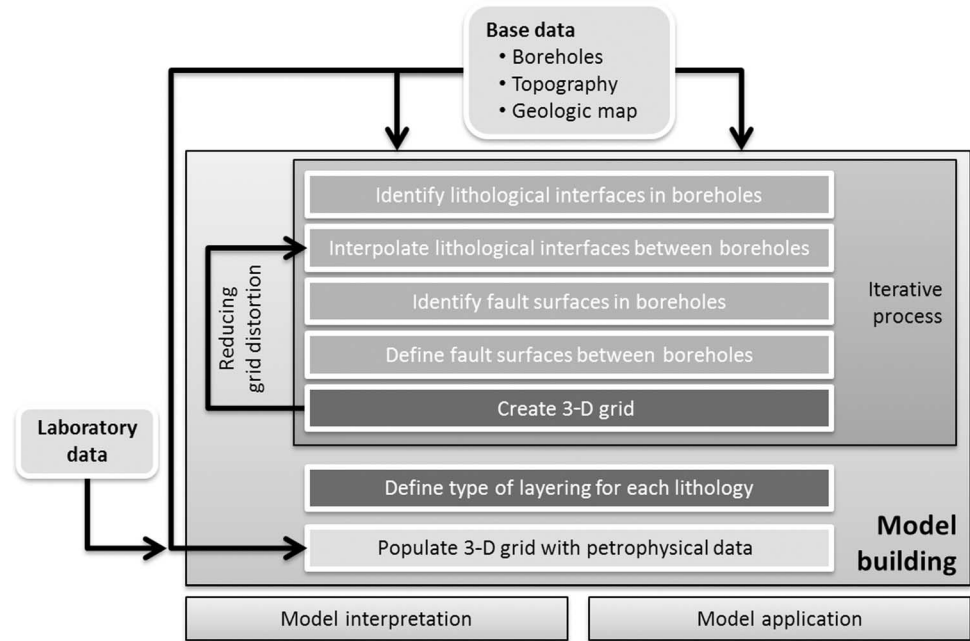

seismic sections. After that, the lithologic interfaces (or seismic interfaces) are traced in the sections and interpolated into the 3-D space respecting the offsets on the faults (see, for example, Dubrule et al., 1997; Dubrule and Damsleth, 2001; Dubrule, 2003). For model building based on 1-D borehole data alone, this workflow has to be changed (Figure 5) and becomes much more iterative. Because only in rare cases faults can be directly identified in the boreholes, the workflow starts with identifying the lithologic interfaces in the boreholes and interpolating them into the 3-D space. Only after that, can faults be identified based on the distribution of the lithologies in space. The individual workflow steps shown in Figure 5 are described below in more detail.

Lithologic interfaces are reconstructed interpolating the well markers using a minimum curvature algorithm (Smith and Wessel, 1990). This algorithm adapts to variable data distribution densities through converging iterations at successively finer grid resolutions. This way, 2-D grids with a cell size of 50 × 50 m (164 × 164 ft) were generated, each representing a lithologic interface. To avoid possible crosscutting of these interfaces during gridding, control points have to be added to each interface. The obtained lithologic interfaces have a high degree of precision in the area of the gas storage facility, where the boreholes are densely spaced (Figure 6).

Away from the Chémery hill, the wells are sparser, and therefore, the interfaces tend to be smoother, and some detail is lost. Nevertheless, the general trend is preserved. As an additional surface in the 3-D space, the water table was also reconstructed the same way as the lithologic interfaces. This surface can be considered representative for the topmost aquifer, a free-water table with seasonal excursion, which may have an impact on the petrophysical properties of the near-surface layers.

Identifying faults starts with the analysis of the borehole data, where, in some cases, evidences of faults can be found in the lithologic well markers. If no such direct evidence is present, strong well-marker displacements between relatively close boreholes (Figures 6–8) can be used as an indirect indication of faults between the boreholes. In addition, elevation (Figure 6) and edge detection maps for the lithologic interfaces as well as isopach maps for the formations were created to ease the detection of structural anomalies in the data, in particular, localized dip (Figure 7) and thickness variations, which can be indicative of faults (Figures 7, 8). As a general rule, high vertical exaggerations should be avoided for fault detection because they can lead to artifacts such as very low–angle faults after removing the exaggeration. In the Chémery area, the Upper Cretaceous chalk
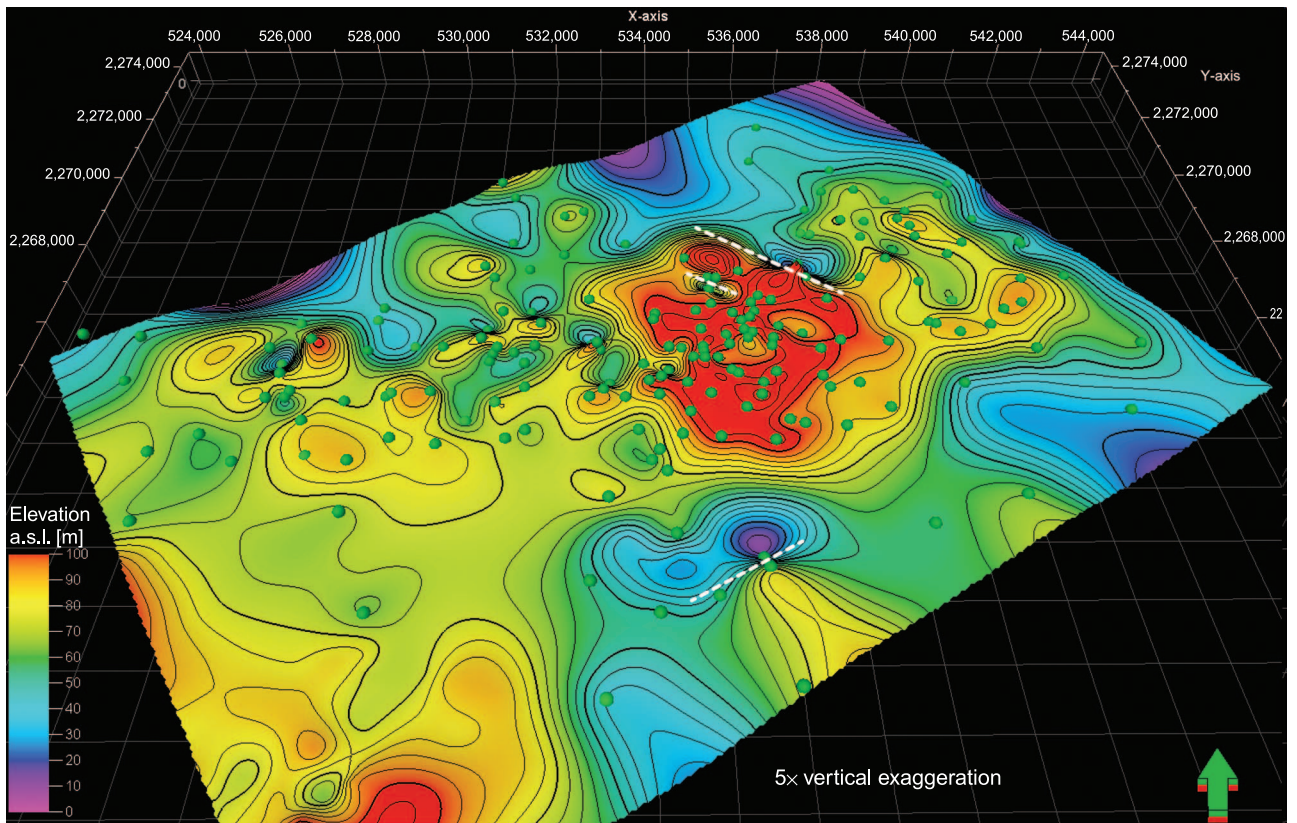
Figure 6. Oblique view of the top Cretaceous interface. Colors represent the elevation above sea level (a.s.l.) of the interface; dots represent the original well markers. The Chémery hill is clearly visible in the Cretaceous strata, slightly northeast of the model center (reddish). Large elevation differences of the interface indicate faults, a few of which are indicated by white dashed lines in the southeast of the model or northeast of the Chémery hill.

proved to be the best marker for detecting faults (Figure 6).

Figure 7 shows the lithologic interfaces and a cross section before and after fault interpretation. Adding the detected faults with their corresponding displacement to the 3-D model reduces the curvature and dip of the lithologic interfaces adjacent to the fault. Therefore, modeling faults strongly influences the reconstruction of the lithologic interfaces. The best results were obtained when both tasks were performed simultaneously with the 3-D grid construction (see below) as an iterative process. To validate the propagation of the fault planes in the 3-D space, their orientations were cross-checked with literature data of local and regional trends in the Paris Basin. For example, some of the deeper faults highlighted in two depth maps (Fleury et al., 1997) with the position of a fault system affecting the reservoir levels and the Cretaceous levels correspond to a set of the modeled near-surface faults.

This observation confirms the model accuracy. After comparing the model with the literature, the fault surfaces were extended to above the top and below the bottom of the model to facilitate the 3-D grid construction.

Three-Dimensional Grid Construction and Population

Once all model surfaces (i.e., lithologic interfaces and faults) are defined in the 3-D space, a hexahedral 3-D grid can be created. The dimensions of the 3-D grid are defined by the quadrilateral 2-D grids on the lithologic interfaces and by the vertical layering. The 3-D grid is created in such a way that lithologic interfaces, fault surfaces, and model boundaries coincide with cell boundaries. Because the data types are differently and unevenly distributed in space, the resulting 3-D grid can have varied spacing. For example, around the Chémery hill, a clustering of

Figure 7. Dip angle (colors) of the upper lithologic interface of the Upper Cretaceous White Chalk with Flints draped on the same interface before (A) and after (B) fault modeling. In the front, a vertical cross section shows some lithologic interfaces, with the top White Chalk with Flints indicated in black in panel B. In panel A, intersections of the future faults with the cross section are indicated as red lines; in panel B, faults are indicated as red surfaces. Black vertical lines are boreholes with dots representing lithologic well markers with the colors defined in Figure 2 and in the legend in panel A. For visualization reasons, Petrel unifies the top White Chalk with Flints and the faults into a single surface. Therefore, high dip angle values close to faults in panel B are not part of the top White Chalk with Flints and should not be considered. SSS = Sand and Shale of Sologne; FDT = Faluns de Touraine; SMOB = Sand and Marl of Orléans and Blois; BEAU = Beauce Limestone; CDF = Continental Detrital Formation; CF = Clay with Flints; WCF = White Chalk with Flints; TJT = Tuffeau Jaune de Touraine; TB_IC = Tuffeau de Bourré and Inocerames Chalk.
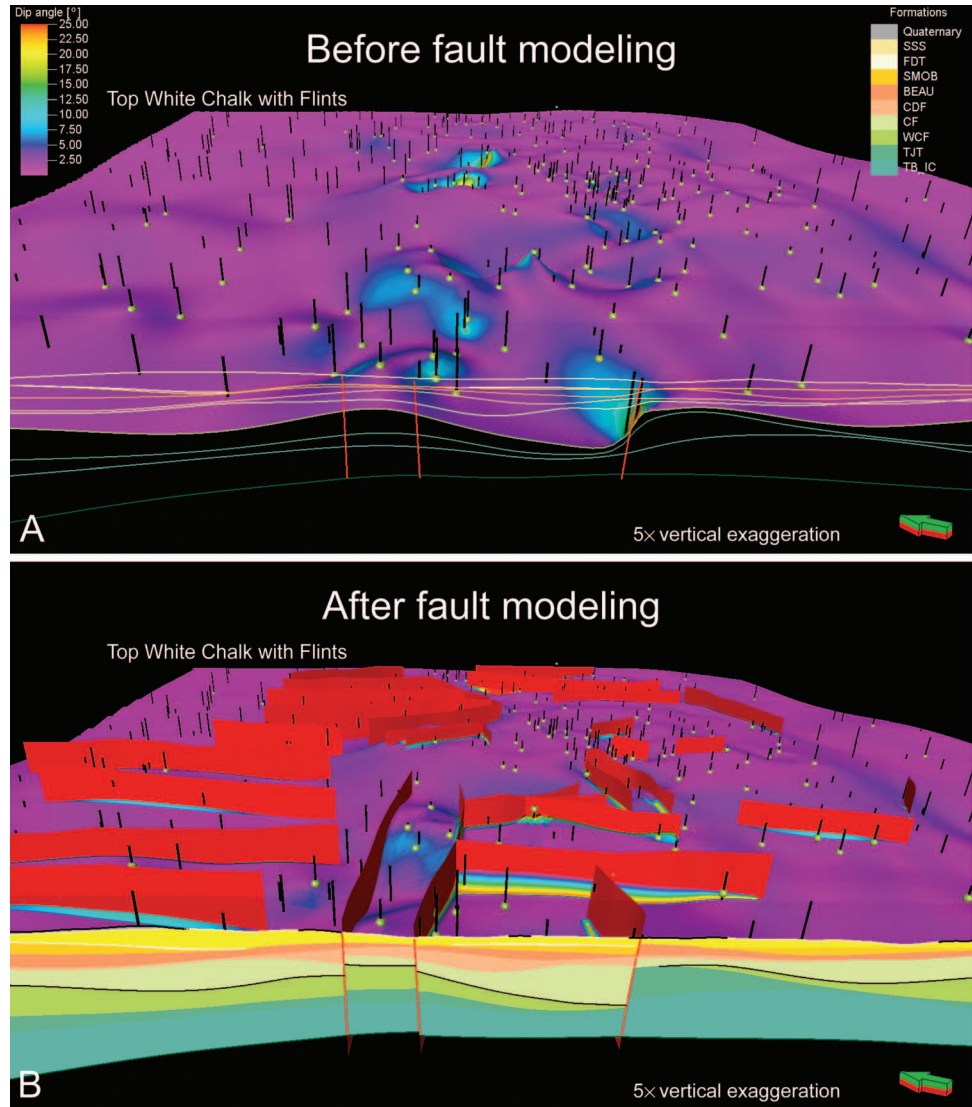
geologic borehole information exists, whose density decreases away from the gas storage facility. However, uphole survey data (i.e., velocity logs) are lacking at the Chémery hill. The vertical distribution of the data also depends on the different data types: the velocity logs have a minimum vertical resolution of 2 m (7 ft), whereas the lithologic well markers have a resolution of approximately 50 cm (20 in.). Therefore, it is necessary to have a grid resolution accommodating these differences in sampling spacing.

To each lithology, a layering is assigned (Figure 9). This layering may have different geometrical properties in each lithology, for example, parallel to the upper or lower lithologic interface, horizontal, or dividing the lithology into a constant number of sublayers (i.e., proportional layering). Assigning the layering requires some geologic background knowledge. For example, a horizontal layering is assigned to the Beauce Limestone (Figure 9) because it consists of lacustrine sediments, which can be assumed to have been deposited horizontally. The horizontal layering also leads to an onlap relationship with the underlying sediments around the Chémery hill as observed in a cross section from Fleury et al. (1997). For the Cretaceous units and the fluvial formations, a proportional layering is assumed; for the Continental Detrital Formation and the Faluns de Touraine, a base-parallel layering is assumed.
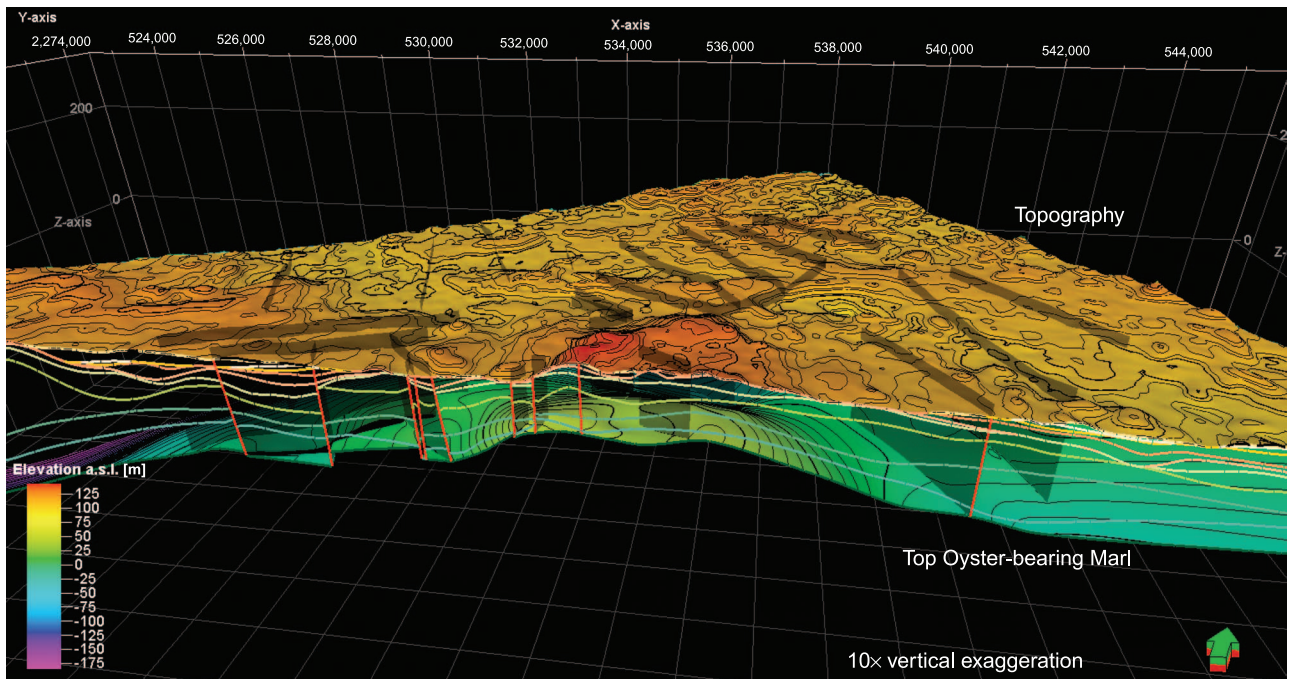
Figure 8. Oblique view of all lithologic interfaces with the topography on top crosscut by a vertical cross section. Colors of the model top and bottom represent elevation above sea level (a.s.l.). Colors of the lithologic interfaces represent the different lithologies according to Figure 2. High curvatures of the lithologic interfaces, for example, the top Cenomanian Oyster-bearing Marl in the model center, can be indicative for faults.

As the final step of the model building, the 3-D grid is populated with the available geologic and petrophysical data from the boreholes such as facies, mineral components, seismic velocity, porosity, or water saturation. The propagation of these properties from the 1-D boreholes into the 3-D grid follows the aforedefined layering in each lithology. Because the data spacing in the boreholes is generally smaller than the 3-D grid spacing, more than one data point per grid cell is present. Various averaging methods can be applied in Petrel to perform the necessary upscaling of the borehole data, for example, arithmetic averaging, volume-weighted averaging, or picking of the majority. The choice of the averaging method depends on the physical property to be upscaled, and two or more properties can be upscaled in a combined manner, for example, one property being the weight of the other property. Once the properties have been upscaled, a geostatistical data analysis is performed; horizontal and vertical variograms are computed for each formation, and the output parameters are used as input of the kriging algorithm (Krige, 1951) to interpolate the property in the 3-D space.

LABORATORY VELOCITY MEASUREMENTS

The BRGM online repository provides P-wave borehole velocity logs. To better constrain the 3-D model and to evaluate the shear-wave velocities (V_S) of the lithologies, longitudinal and transversal wave speeds as well as porosity and density were measured. We collected 25 suitable rock samples, representative of the lithologies in the 3-D geologic model, from 53 outcrops between the villages of Chémery, Cheverny, and Montrichard (see Figure 1). The 25.4-mm diameter and 30- to 50-mm length cylindrical samples were obtained by drilling core plugs directly from the samples. The ends of the plugs were ground with a rotating diamond plate to meet the required planarity and parallelism between the two ends, which can be estimated to be approximately ±10 μm.
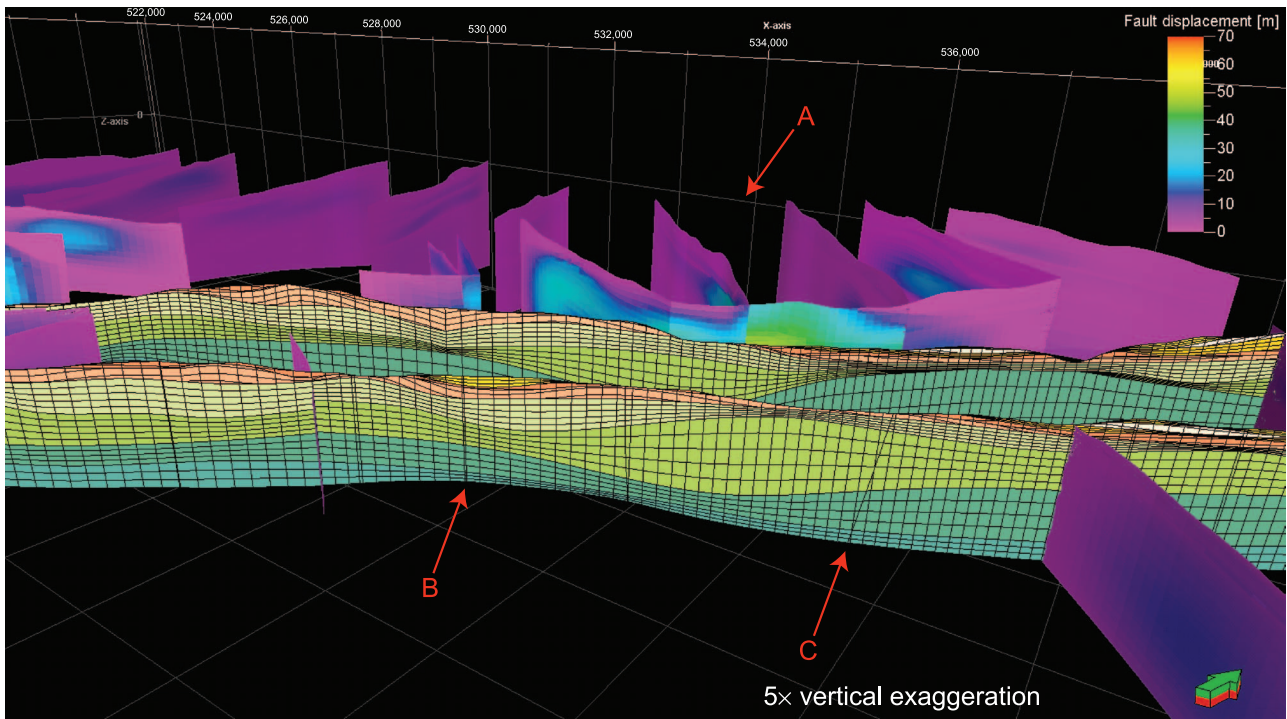
Figure 9. Oblique view of the final lithologic model. Colors represent lithology according to Figure 2. Fault surfaces are displayed with their respective displacement. Note that each lithology has an individual layering assigned to it indicated by continuous black lines. The cross section in the back follows one section of the three-dimensional grid and is therefore curved where the grid is distorted. The cross section in the front is straight and intersects the distorted three-dimensional grid. The arrow in the back (A) points to a horst and graben system, where the displacement maximum is close to the cross section (and close to the Chémery hill) and diminishes away from the Chémery Hill. The left red arrow (B) highlights a location of two very closely spaced grid intersections. The right red arrow (C) highlights a grid intersection, where the grid is strongly distorted.

To calculate the density (ρ), the volume (V) was determined for each plug, measuring the dimensions of the rock cylinder with a 10-µm precision caliper, as well as the mass in dry conditions (m_d) by means of a 1-mg precision scale. The porosity of the samples (ϕ) was measured using a helium pycnometer (Micromeritics AccuPyc 1330) (Figure 10).

Since the studied lithologies are from shallow formations with a maximum depth of 190 m (623 ft) corresponding to a maximum confining pressure of 4.3 MPa (623.7 psi; considering a lithostatic pressure gradient of 22.7 kPa/m [3.3 psi/ft]), both P- and S-wave speed measurements in unconfined and dry conditions were conducted as a first approximation. Subsequently, the samples were saturated with freshwater, and wave speeds were measured under unconfined and wet conditions. These latter measurements can estimate how

groundwater influences the physical properties of the lithologies. Saturation was obtained keeping the samples under vacuum and submerged in the water for 3 to 4 days. After measuring the mass of the saturated sample (m_s) the degree of saturation (S_d) can be calculated as

$$S_d\ (\%) = 100\frac{m_s - m_d}{\phi \rho_w V} \qquad (1)$$

where ρ_w is the density of water. The applied saturation procedure resulted in a saturation of more than 90% for all samples.

The velocity measurements were performed at the Rock Deformation Laboratory at ETH Zurich using the pulse-transmission method (Birch, 1960) (Figure 10). To measure transversal and longitudinal wave speeds, the samples were placed between two ultrasonic transducers, the first acting as the emitter, and the second as the receiver. A good coupling
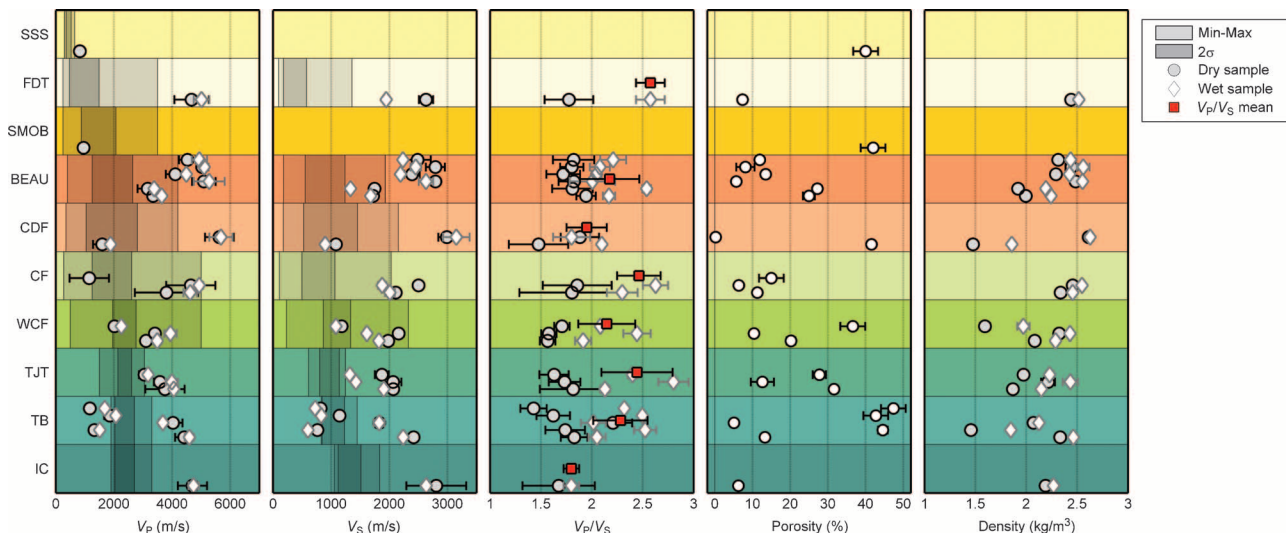
Figure 10. Laboratory measurements of P- and S-wave velocity in dry and fully water-saturated state, resulting V_P/V_S ratios, porosity, and density. Shaded areas in the plot represent the borehole-derived V_P model and the synthetic V_S model derived from the application of the V_P/V_S ratio of the wet measurements (red squares), respectively. Some P-wave velocity measurements in wet conditions and some S-wave velocity measurements failed because of the unconsolidated state of the rock samples. SSS = Sand and Shale of Sologne; FDT = Faluns de Touraine; SMOB = Sand and Marl of Orléans and Blois; BEAU = Beauce Limestone; CDF = Continental Detrital Formation; CF = Clay with Flints; WCF = White Chalk with Flints; TJT = Tuffeau Jaune de Touraine; TB = Tuffeau de Bourré; IC = Inocerames Chalk. The exact values of the laboratory measurements can be found in the online repository (AAPG Datashare 49 at www.aapg.org/datashare).

between the sample faces and the transducers was obtained by placing ultrasonic coupling gel between the interfaces and by compressing the sample-transducers assembly in a small bench screw press. The pulse generator (Matec TB1000), mounted on the personal computer (PC), provided to the emitter 0.25-MHz frequency sinusoidal pulses of 20-μs duration and 13-ms repetition rate. Seismic signals from the receiver were acquired using a digital oscilloscope (LeCroy Waveace 214). To increase the signal-to-noise ratio, 256 subsequent pulses were stacked for each measurement. The trigger was provided by the pulse generator, and the oscilloscope was connected to the acquisition PC via a local area connection (LAN). The digital traces were directly uploaded through the LAN to the PC governed by an ad-hoc written Matlab routine. The delay introduced by all the elements, which are not the sample, such as the material between the piezo-electric element and the outer face of the transducer, was measured using a standard calibration procedure (Prelicz, 2005; Ferri et al., 2007).
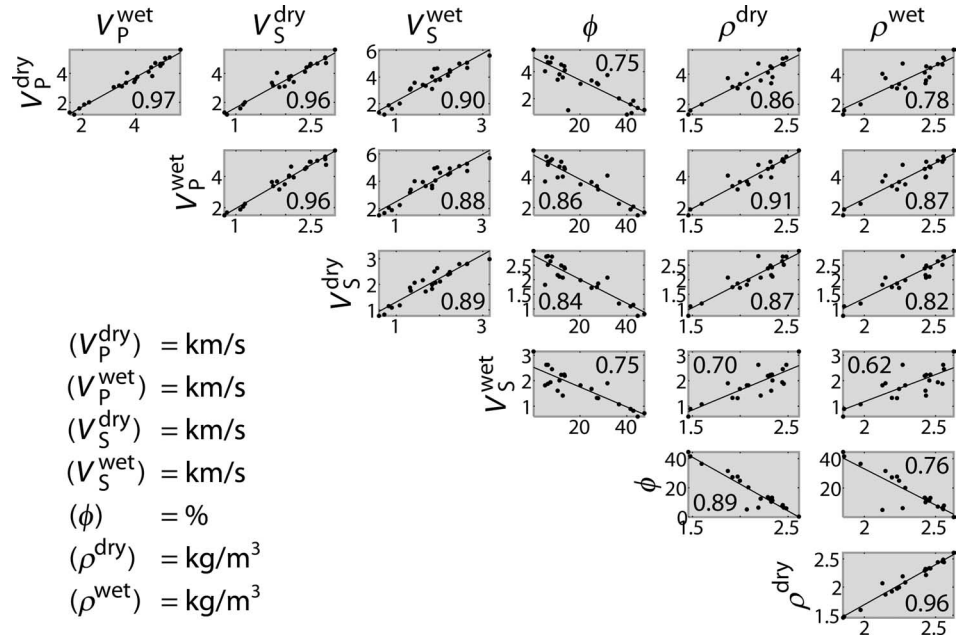
The correlations between the different laboratory measurements are shown as crossplots in Figure 11. Coefficients of determination, R^2, are generally relatively high, suggesting that most measured parameters depend on each other. As a first approximation, it can be assumed that the V_P/V_S ratio measured at 0.25 MHz is similar to the ratio measured at the frequency of the BRGM borehole velocity logs. Therefore, V_S can be calculated from the V_P data provided by the BRGM borehole velocity logs, and a shallow 3-D V_S model can be built. A correction of laboratory measurements to in-situ values could be applied to intervals deeper than 50-m (164-ft) depth (Urmos et al., 1993), but is out of the scope of this article.

MODELING RESULTS, ANALYSIS, AND INTERPRETATION

The full final model (Figures 9, 12) can be downloaded from the journal online repository (AAPG Datashare 49 at www.aapg.org/datashare) as a Petrel project (Schlumberger). The same model, limited to lithologic interfaces and faults, is available online as a Move project (Midland Valley). The coordinate system of the model is

Figure 11. Crossplots of laboratory measurements (Figure 10) of P-wave velocity (V_P), S-wave velocity (V_S), and density with their respective coefficients of determination, R^2. Each point represents a data couple derived from the same sample. Units of the various measurements are given in the figure.

$$(V_P^{dry}) = km/s$$
$$(V_P^{wet}) = km/s$$
$$(V_S^{dry}) = km/s$$
$$(V_S^{wet}) = km/s$$
$$(\phi) = \%$$
$$(\rho^{dry}) = kg/m^3$$
$$(\rho^{wet}) = kg/m^3$$

NTF France II, which is also used in all figures except for Figure 1.

Lithologies and Their Interfaces

Few Turonian lithologic well markers were present in the boreholes. Based only on few data points, it was possible to reconstruct the top lithologic interfaces of the Tuffeau Jaune de Touraine and the Tuffeau de Bourré, but not the interface between the Tuffeau de Bourré and the lowermost Turonian formation, the Inocerames Chalk, which were therefore modeled as one unit. Given the low data density, the resulting Turonian interfaces are very smooth, and they do not show particular displacements (Figure 12A). However, similar to the younger formations, they are uniformly deformed in the dome structure below the Chémery hill (Figure 8).

The modeling of the lithologic interfaces shows very good results for the lithologies with dense borehole data such as the Upper Cretaceous White Chalk with Flints and the Clay with Flints. These formations are uniformly present throughout the entire study area and are folded and partly outcropping in the dome structure at the Chémery hill. The geometry of these Upper Cretaceous formations is complex, and they show important thickness variations resulting from postdepositional alteration

processes such as dissolution, which led to the formation of solution pipes and to the development of karst systems. In some cases, karst features led to the passive deformation of the overlying formations. Vertical displacement of the formations can be recognized from the elevation differences of the lithologic well markers between neighboring boreholes, which allow interpreting the offset on fault planes (Figure 12A). These Upper Cretaceous formations exhibit a top interface characterized by domes and depressions. Locally, elevation differences of as much as 20 m (ft) are present in these formations, indicating offsets along faults. Whereas small-scale undulations can be indicators of fault displacements, higher amplitude features represent major scale folding.

The dome and depression geometry is common to most of the chalks in the southeastern Paris Basin (Hanot and Renoux, 1991; Hanot and Thiry, 1999). The depressions on top of the Clay with Flints are commonly filled with the overlying Continental Detrital Formation (Figure 12A). In the model, this formation is well constrained by a high density of lithologic well markers at the Chémery hill and in smaller areas southwest and northeast of the hill. The presence of this formation in areas away from the Chémery hill could be explained by erosion from the topographic high and redeposition as colluvium in topographic depressions. In some rare
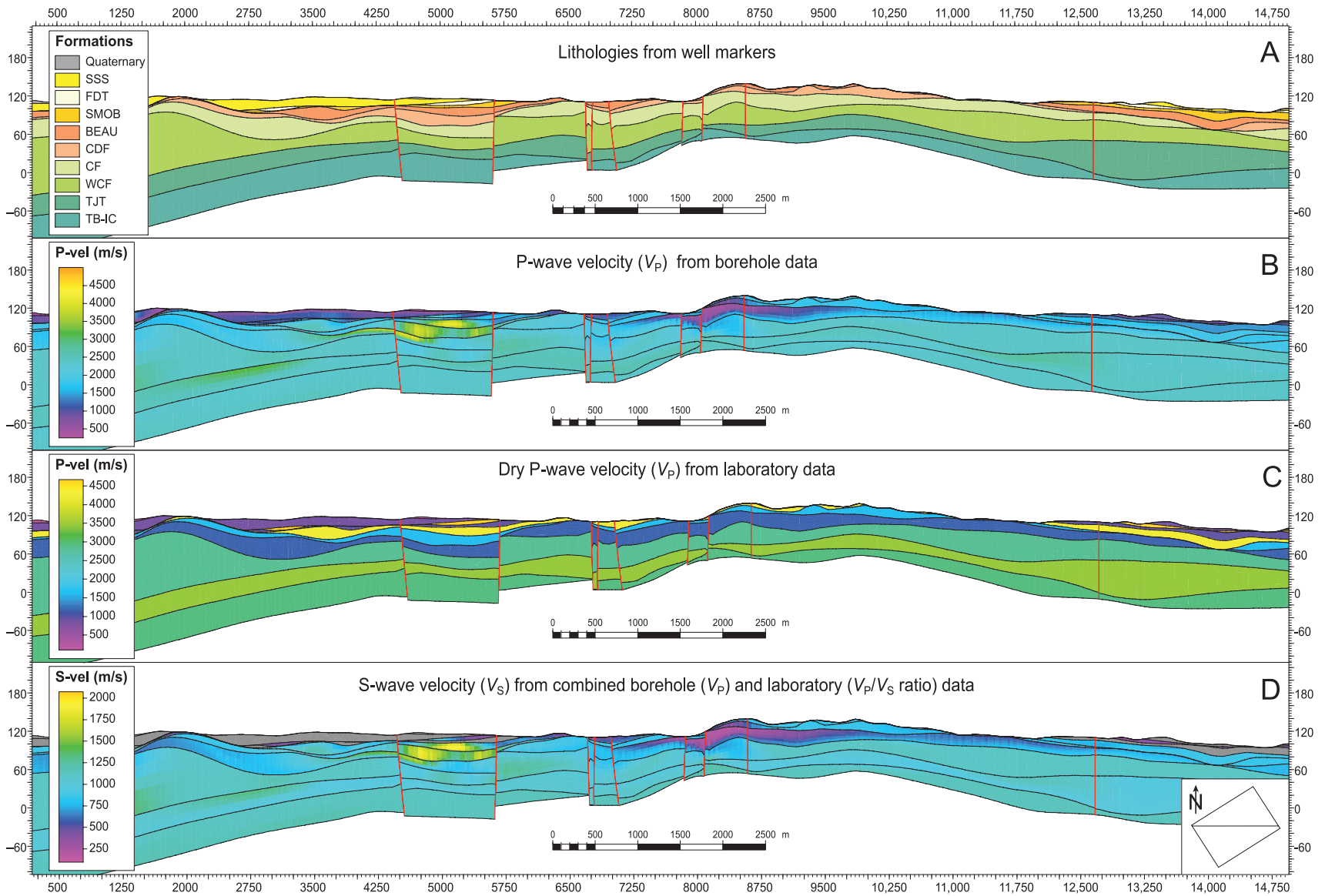
Figure 12. Cross sections through the final three-dimensional model showing the lithology from the borehole lithologic well markers (A), the P-wave velocity from the uphole seismic survey data (B), the dry P-wave velocity from the laboratory measurements (C), and the experimental S-wave velocity derived from the application of the wet V_P/V_S ratio (D). Formation abbreviations in the legend in panel A are the same as those in Figure 7. All four cross sections are located at the same place in the model indicated in the inset showing the model boundaries in map view. Horizontal coordinates indicate length in meters along the cross sections with arbitrary origin. V_p = P-wave velocity; V_s = S-wave velocity.

cases, the redeposited Continental Detrital Formation is even overlying the more recent lacustrine Beauce Limestone. In fact, the Beauce Limestone can be topographically lower than the Continental Detrital Formation, filling a small depression on the southeastern side of the Chémery hill. Small interfingering of Beauce Limestone in a normal sequence is also present in a limited amount on the top of the hill. In general, the lacustrine limestones are present more or less continuously across the whole model area and seem to seal an early Tertiary paleotopography, represented by the top of the Clay with Flints and the top of the Continental Detrital Formation. North of the Chémery hill, the Miocene marine formations of the Faluns de Touraine are deposited in a narrow band eroding the Sand and Marl of Orléans and Blois.

Some of the Cenozoic lithologic well markers show sparse data clusters (e.g., the Continental Detrital Formation or the Faluns de Touraine sands), whereas others exhibit a more continuous distribution across the study area (e.g., the Sologne Sand and Shale). The fluvial and lacustrine formations encircle the Chémery hill without covering it, with the exception of the lacustrine Beauce Limestone, which partially covers the southeastern side of the hill.

Structural Analysis

Based on the analysis of dip angle maps, thickness maps, and cross sections, several fault systems affecting the uppermost formations can be identified in the model (Figures 9, 12). These fault systems are mostly oriented north–south and west–east and correlate with the fault systems identified by Fleury et al. (1997) (Figure 1) in two depth maps at the Upper Triassic and Lower Jurassic reservoir levels and at the Cretaceous levels. This correlation suggests that at least parts of the near-surface fault network are related to a reactivation of older faults during the Cenozoic. In fact, some of these faults can be traced from the Cenomanian formations up to the surface.

North of the Chémery hill, the 3-D fault network exhibits a distinct horst and graben structure indicating an east–northeast to west–southwest extension (back of Figure 9 denoted as A). The displacement

maximum of as much as 60 m (197 ft) is close to the cross section in the back of Figure 9, that is, very close to the Chémery hill, and it decreases abruptly away from the hill. This structure can also be recognized in cross-sectional view, where thickness variations and sudden changes in the dip angle of the lithologies allow recognition of tectonic influences, which can be discriminated from sedimentary features.

Below the Chémery, hill a dome structure reveals itself in the 3-D geologic model. This dome probably originates from one of the several tectonic pulses that affected the Paris Basin in the Paleogene. The onlap relationship of the post-Eocene formations (Beauce Limestone and Sand and Marl of Orléans and Blois) on top of the Upper Cretaceous formations (Clay with Flints and White Chalk with Flints) suggests that a paleotopographic high already existed in the Early Cenozoic, when the exposed White Chalk with Flints was altered in situ and strong siliceous crusts developed under humid climatic conditions.

Velocity Modeling

The 3-D V_P model reconstructed from the borehole velocity logs (Figure 12B) shows a constant increase of the velocity with depth with some localized velocity inversions. These anomalies are concentrated in the Beauce Limestone, the Continental Detrital Formation, the White Chalk with Flints, and the lower Turonian chalks. The post-Miocene formations representing the uppermost layers of the model exhibit very low velocities of approximately 800 m/s (2625 ft/s). Immediately below the Sand and Marl of Orléans and Blois, the Beauce Limestone shows velocity values of approximately 3000 m/s (9843 ft/s). On average, the Continental Detrital Formation shows low velocities combined with localized peaks of high velocities of as much as 5000 m/s (16,404 ft/s). Local velocity anomalies are also characteristic for the Clay with Flints. A fast-slow-fast velocity sequence is detected in the Upper Cretaceous interval, that is, the White Chalk with Flints–Tuffeau de Touraine–Tuffeau du Bourré and Inocerames Chalk intervals.

Figure 10 offers a synoptic view at the formation level of the experimental longitudinal (V_P) and

transversal (V_S) wave speeds and their associated error bars, compared with the borehole-derived values. The latter correspond to the shaded areas in Figure 10; the lighter representing the minimum and maximum range of the model, the darker, the standard deviation (σ) range. The dry V_P values range between 828 m/s (2717 ft/s; Sologne Sand and Shale) and 5627 m/s (18,461 ft/s; Continental Detrital Formation, silicified facies), whereas the saturated values range from 1516 m/s (4974 ft/s; Tuffeau de Bourré) to 5105 m/s (16,749 ft/s; Continental Detrital Formation). The dry V_S values range between 763 m/s (2503 ft/s; Tuffeau de Bourré) and 2989 m/s (9806 ft/s; Continental Detrital Formation, silicified facies), the saturated values between 726 and 3152 m/s (2382 and 10,341 ft/s). Porosities range between 0.22% (Continental Detrital Formation, silicified facies) and 47.37% (Tuffeau de Bourré). Density ranges between 1.4 and 2.7 kg/m^3.

DISCUSSION

Standard geologic modeling based on seismic 2-D sections or 3-D cubes is quite different to the modeling presented here based solely on 1-D borehole data and laboratory wave speed measurements. The type of data requires a different workflow (Figure 5), starting with the identification of lithologic interfaces in the borehole lithologic well markers and interpolation of these interfaces into the 3-D space. Only after this step, can fault planes be identified based on the 3-D geometry of the lithologic interfaces. This part of the presented workflow is opposite to modeling based on 2-D sections, for which faults are commonly identified first on seismic sections before the lithologic (or seismic) interfaces are traced in the 2-D sections and interpolated between them. Also, the workflow presented here is much more iterative and time-consuming, meaning that the described steps have to be performed several times in a loop (Figure 5) to attain a satisfactory 3-D modeling result. The circumstance that seismic sections are rarely publicly available while borehole data can be found more easily, thanks to the databases of national geologic surveys (e.g., BRGM in France), makes the presented workflow valuable for geologic modeling based on public data. It was successfully demonstrated that a robust geologic 3-D near-surface model based only on borehole data is feasible. Such a model provides additional information about the study area, for example, by putting in evidence the paleotopography and highlighting the angular unconformity on top of the White Chalk with Flints formation, which is delineated by karst features, by Eocene detrital filling, and sealed by the deposition of Oligocene–Miocene lacustrine limestones.

Only very few fault planes can be recognized directly in the lithologic well logs. Most faults are interpreted from curvature maps, dip angle maps, and strong vertical elevation differences of individual lithologies between neighboring boreholes. Therefore, modeling of fault planes is substantially different compared to modeling based on 2-D seismic sections, in which the fault planes can be identified directly in the base data. In the presented model, not only the exact position, but also the dip direction and dip angle of fault planes, commonly have to be defined interpretatively between boreholes. Nevertheless, the good correlation between the modeled near-surface faults and the deeper faults mapped by Fleury et al. (1997) and shown in Figure 1 underlines the robustness of the model and of the applied modeling workflow. Accurately modeling faults is essential from a commercial point of view because the near-surface faults may be linked to the deeper structures in the reservoir. Knowing their position can help the storage managers to monitor possible gas leakages.

Depending on the geologic complexity of the study area (e.g., fault density and geometry or amount and deformation of lithologies), the 3-D grid may become quite strongly distorted during gridding. A too strongly distorted grid is undesirable because its population with petrophysical data becomes inaccurate. The Petrel software offers various options to minimize the grid distortion, but a completely undistorted grid is impossible to attain because it is forced to follow the lithologic interfaces and fault planes. In the final model, two possibilities exist for visualizing cross sections (Figure 9): (1) following

the distorted grid and (2) straight cross section intersecting the distorted grid. The first option (cross section in the back in Figure 9) has the disadvantage that the cross section is not necessarily straight, depending on the degree of distortion of the 3-D grid. Also, the grid intersections can only be visualized in two orthogonal directions predefined by the hexahedral grid. The second option (cross section in the front in Figure 9) has the advantage of being straight. However, the intersection with the distorted 3-D grid can lead to crosscutting artifacts (highlighted as B and C in Figure 9), which may lead to misinterpretations. Such artifacts are not present in the first option cross sections. Which option is best for a specific model depends on the grid distortion and the desired cross-sectional orientation.

The comparison between laboratory and field velocity data (Figures 10, 12) must consider the error of the measurements, the weathering conditions of the samples, the proximity to a fault damage zone (i.e., fracturing of the rock), and the different pressure conditions and frequency ranges at which the data were acquired. In addition, the laboratory measurements were preferentially performed on highly consolidated samples to avoid failure of the core plugs. This can lead to wave speeds slightly higher than the expected values from the borehole data (Figure 10). However, the experimental values are compatible with the borehole observations, falling for almost all cases in the range of the borehole model and literature data (Castagna et al., 1985; Hanot and Thiry, 1999) Nevertheless, for some formations (Clay with Flints, Beauce Limestone, Faluns de Touraine), laboratory wave speeds cluster at higher values than the borehole values. This can be related to the local variation in the rock texture in combination with diagenetic phenomena such as cementation, recrystallization, and silicification, which lead to porosity reduction altering the elastic moduli of the rock (Hanot and Thiry, 1999; Eberli et al., 2003; Fabricius, 2003; Røgen et al., 2005; Fabricius et al., 2008). Saturated samples have generally higher V_P than the dry samples, while, at the same time, their V_S is lower than the V_S measured in dry samples. This behavior can be explained for wet conditions with the increasing of effective bulk modulus (i.e., the pores are filled with water instead of air), which leads to an increase of V_P and an increase of density, which results in a decrease of V_S (e.g., Miller and Stewart, 1991; Cadoret et al., 1992). In the final model (Figure 12), the borehole-derived velocity model has a finer resolution than the laboratory-derived model because the latter attributes a single averaged value of a representative sample to an entire formation. Nevertheless, the laboratory-derived model is of utmost importance because it provides the V_P/V_S ratio, which can be used to transform the borehole V_P into a V_S model (Figure 12D).

CONCLUSIONS

Geologic near-surface modeling solely based on 1-D borehole data is considerably more challenging than modeling based on seismic 2-D sections or 3-D cubes because of the amount of interpretative effort. Nevertheless, it is also a faster and cheaper procedure to unravel the shallow subsurface considering the ready accessibility of borehole data from public domain repositories, unlike the acquisition of near-surface seismic data. Because fault surfaces are difficult to directly identify in the boreholes, they commonly have to be interpreted between the boreholes based on the modeled lithologic interface geometries. A new and more iterative workflow is presented to achieve a robust geologic model in the Chémery area. Naturally, in areas with higher borehole data density (e.g., in the gas storage facility area), the final model is not only more accurate, but also more delicate to build. In areas with lower data density (e.g., in the deeper parts of the model or away from the gas storage facility), the model is smoother. Generally, the good correlation between the modeled shallow faults and known deeper faults demonstrates the high accuracy achievable with geologic modeling based on borehole data.

Populating the 3-D model grid with petrophysical data (either from boreholes or from laboratory testing) reveals, for example, the shallow 3-D seismic velocity structure or the 3-D porosity field. The near-surface low-velocity layer can easily be identified in the model. In addition, the model reveals various important velocity inversions, the most

significant one localized in the Beauce Limestone and a second one in the White Chalk with Flints. Laboratory P- and S-wave velocity measurements complement the model and are used to populate the 3-D model grid in addition to the borehole data and enrich the information content of the model, for example, by adding meaningful V_P/V_S ratios to all lithologies.

The 3-D shallow geologic model allows drawing two major structural conclusions in the study area. First, the dome structure that expresses itself on the surface of the Earth as the Chémery hill is also present in deeper lithologic levels. The Upper Cretaceous formations also follow the dome shape at depth, and the onlap relationship of the post-Eocene units around the Chémery hill suggests that a topographic high was already present at the beginning of the Cenozoic. Second, thickness variations in the modeled formations indicate that some of the older Triassic faults were reactivated during the deposition of the Beauce Limestone and later formations. Some of these faults can be traced all the way up to the surface of the Earth.

REFERENCES CITED

Beccaletto, L., F. Hanot, O. Serrano, and S. Marc, 2011, Overview of the subsurface structural pattern of the Paris Basin (France): Insights from the reprocessing and interpretation of regional seismic lines: Marine and Petroleum Geology, v. 28, p. 861–879.

Birch, A. F., 1960, The velocity of compressional waves in rocks to 10 kilobars: Part 1: Journal of Geophysical Research, v. 65, p. 1083–1102, doi:10.1029/JZ065i004p01083.

BRGM, 2010, InfoTerreTM, http://infoterre.brgm.fr/.

Burtscher, A., M. Frehner, and B. Grasemann, 2012, Tectonic geomorphological investigations of antiforms using differential geometry: Permam anticline, northern Iraq: AAPG Bulletin, v. 96, p. 301–314, doi:10.1306/06141110204.

Cadoret, T., D. Marion, and B. Zinszner, 1992, Sonic wave velocity and x-ray tomography images for partially saturated rocks: Evidence of microscopic fluid distribution effect on acoustic properties: 3rd European Core Analysis Symposium of the Society of Core Analysts, Paris, France, September 1992, p. 275–291.

Castagna, J. P., M. L. Batzle, and R. L. Eastwood, 1985, Relationships between compressional-wave and shear-wave velocities in clastic silicate rocks: Geophysics, v. 50, p. 571–581, doi:10.1190/1.1441933.

Cox, M. J. G., 1999, Static corrections for seismic reflection surveys: Society of Exploration Geophysicists Geophysical References Series 9, 546 p.

Debeglia, N., and S. Debrand-Passard, 1980, Principaux accidents tectoniques issus des corrélations entre les données géophysiques et les données de terrain dans le sud-ouest du Bassin de Paris: Bulletin de la Société Géologique de France, v. 22, p. 639–64.

Dessandier, D., H. Gaboriau, P. Le Berre, L. Rasplus, and M. Rautureau, 1996, Petrophysical properties of the Tuffeau Blanc de Touraine: Application to the durability of building stones: Chronique de la Recherche Minière, v. 64, p. 3–14.

Dubrule, O., 2003, Geostatistics for seismic data integration in Earth models: Society of Exploration Geophysicists Distinguished Instructor Series 6, 279 p.

Dubrule, O., and E. Damsleth, 2001, Achievements and challenges in petroleum geostatistics: Petroleum Geoscience, v. 7, p. S1–S7, doi:10.1144/petgeo.7.S.S1.

Dubrule, O., C. Basire, S. Bombarde, P. Samson, D. Segonds, and J. Wonham, 1997, Reservoir geology using 3-D modeling tools: Society of Petroleum Engineers Annual Technical Conference and Exhibition, San Antonio, Texas, October 5–8, 1997, SPE 38659, 16 p., doi:10.2118/38659-MS.

Eberli G. P., G. T. Baechle, F. S. Anselmetti, and M. L. Incze, 2003, Factors controlling elastic properties in carbonate sediments and rocks: The Leading Edge, v. 22, p. 654–660, doi:10.1190/1.1599691.

Fabricius, I. L., 2003, How burial diagenesis of chalk sediments controls sonic velocity and porosity: AAPG Bulletin, v. 87, p. 1755–1778, doi:10.1306/06230301113.

Fabricius, I. L., L. Gommesen, A. Krogsbøll, and D. Olsen, 2008, Chalk porosity and sonic velocity versus burial depth: Influence of fluid pressure, hydrocarbons, and mineralogy: AAPG Bulletin, v. 92, p 201–223, doi:10.1306/10170707077.

Ferri, F., L. Burlini, B. Cesare, and R. Sassi, 2007, Seismic properties of lower crustal xenoliths from El Hoyazo (SE Spain): Experimental evidence up to partial melting: Earth and Planetary Science Letters, v. 253, p. 239–253, doi:10.1016/j.epsl.2006.10.027.

Fleury, R., 1997, Carte géologique de la France (1/50,000), feuille Romorantin (460): Orléans, France, Bureau de Recherches Géologiques et Minières, 1 sheet.

Fleury, R., F. Charnet, J. Corpel, S. Debrand-Passard, Y. Gros, and P. Maget, 1997, Notice explicative, carte géologique de la France (1/50,000), feuille Romorantin (460): Orléans, France, Bureau de Recherches Géologiques et Minières, 94 p.

Fritsche, S., and D. Fäh, 2009, The 1946 magnitude 6.1 earthquake in the Valais: Site effects as contributor to the damage: Swiss Journal of Geosciences, v. 102, p. 423–439, doi:10.1007/s00015-009-1340-2.

Grauls, D., and P. Lafay, 1979, Le reservoir gréseux du Trias: Terminal de la structure de Contres-Chémery—Exemple de description sédimentologique base sur l'analyse litho-diagraphique: Revue de l'Institut Français du Pétrole, v. 34, p. 67–82.

Hamon, Y., and G. Merzeraud, 2005, Nouvelles données sur le Trias de Sologne (Chémery, sud-ouest du Bassin de Paris): Stratigraphie et environnements de depots: Géologie de la France, v. 1, p. 3–22.

Hanot, F., and P. Renoux, 1991, Petrophysical variations in the Senonian chalk of the Paris Basin and their influence on static corrections: First Break, v. 9, p. 515–526.

Hanot, F., and M. Thiry, 1999, Anomalies sismiques dans la craie et deformations superposes dans les formations tertiares du sud-est du Bassin de Paris: Bulletin de la Société Géologique de France, v. 170, p. 915–926.

Havenith, H.-B., D. Fäh, U. Polom, and A. Roullé, 2007, S-wave velocity measurements applied to the seismic microzonation of Basel, Upper Rhine Graben: Geophysical Journal International, v. 170, p. 346–358, doi:10.1111/j.1365-246X.2007.03422.x.

Huault, V., G. Merzeraud, R. Rauscher, and M. Schuler, 1995, Palynological variations and sedimentary cycles in the Jurassic from the Paris Basin: Review of Palaeobotany and Palynology, v. 87, p. 27–41, doi:10.1016/0034-6667(94)00140-F.

Jarvis, I., and A. S. Gale, 1984, The Late Cretaceous transgression in the SW Anglo-Paris Basin: Stratigraphy of the Villedieu Chalk Formation: Cretaceous Research, v. 5, p. 195–224, doi:10.1016/S0195-6671(84)80019-1.

Krige, D. G., 1951, A statistical approach to some basic mine valuation problems on the Witwatersrand: Journal of the Chemical, Metallurgical and Mining Society of South Africa, v 52, p. 119–139.

Laignel, B., F. Quesnel, R. Meyer, and J.-J. Macaire, 1998, Relations quantitatives entre les craies à silex et les formations résiduelles à silex de l'ouest du Bassin de Paris: Geodinamica Acta, v. 11, p. 171–181, doi:10.1016/S0985-3111(98)80003-X.

Larue, J.-P., and R. Etienne, 1998, Les formations détritiques Miocènes, Pliocènes et Quaternaires entre le Massif Central et la Sologne: Nouveaux elements d'interprétation: Géologie de la France, v. 1, p. 39–56.

Larue, J.-P., and R. Etienne, 2002, Les Sables de Lozère et les Sables de Sologne: Nouvelles interprétations de deux décharges détritiques du Miocène inférieur, issues de la paléo-Loire (Bassin Parisien, France): Bulletin de la Société Géologique de France, v. 173, p. 185–192, doi:10.2113/173.2.185.

Ménillet, F., and N. Edwards, 2000, The Oligocene–Miocene Calcaires de Beauce (Beauce Limestones), Paris Basin, France, in E. H. Garlowski-Kodersch and K. P. Kelts, eds., Lake basins through space and time: AAPG Studies in Geology, v. 46, p. 417–424.

Merzeraud, G., 1992, Géométrie et signification géodynamique des séquences de dépôts en domaine continental et marin restreint: exemple du Lias inférieur, du sud-ouest du Bassin de Paris, (applications aux potentialités de stockages de gaz naturel en nappes aquifères): Ph.D. thesis, Université Louis Pasteur (Université Strasbourg 1), Strasbourg, France, 200 p., http://www.crewes.org/ForOurSponsors/ResearchReports/.

Merzeraud, G., M. Hoffert, F. Verdier, and R. Rauscher, 1999, Architecture et preservation des reservoirs silicoclastiques du Lias inferieur du sud-ouest du Bassin de Paris: Exemple de la structure de stockage Gaz de France de Chemery en Sologne: Bulletin de la Société Géologique de France, v. 170, p. 741–757.

Merzeraud, G., R. Rauscher, M. Hoffert, and F. Verdier, 2000, Mode d'empilement et distorsion de sequencesgenetiques en milieu marin restreint: Facies et architecture des depotshettangiens du sud-ouest du Bassin de Paris: Bulletin de la Société Géologique de France, v. 171, p. 341–353, doi:10.2113/171.3.341.

Miller, S. L. M., and R. Stewart, 1991, The relationship between elastic-wave velocities and density in sedimentary rocks: A proposal, in CREWES Research report, v. 3: Calgary, Consortium for Research in Elastic Wave Exploration Seismology at the University of Calgary, Canada, p. 260–273.

Miller, R. D., J. H. Bradford, and K. Holliger, 2010, Advances in near-surface seismology and ground-penetrating radar: Society of Exploration Geophysicists Geophysical Developments Series 15, 512 p.

Perrodon, A., and J. Zabek, 1990, Paris Basin, in M. W. Leighton, ed., Interior cratonic basins: AAPG Memoir 51, p. 633–679.

Poggi, V., D. Fäh, J. Burjanek, and D. Giardini, 2012, The use of Rayleigh-wave ellipticity for site-specific hazard assessment and microzonation: Application to the city of Lucerne, Switzerland: Geophysical Journal International, v. 188, p. 1154–1172, doi:10.1111/j.1365-246X.2011.05305.x.

Prelicz, R. M., 2005, Seismic anisotropy in peridotites from the Western Gneiss region (Norway): Laboratory measurements at high PT conditions and fabric-based model predictions: Ph.D. thesis, ETH Zurich, Zurich, Switzerland, 138 p.

Prigent, D., 1997, Exploitation et commercialisation du Tuffeau Blanc (XVe–XIXe siècles), in J.-L. Marais, ed., Mines, carriers et societies dans l'histoire de l'ouest de la France: Annales de Bretagne et des Pays de l'ouest 104, p. 67–80.

Rauscher, R., G. Merzeraud, and M. Schuler, 1992, Biostratigraphie, environments et cortèges de depots dans le Lias inférieur de Sologne (S.W. du Bassin de Paris): Review of Palaeobotany and Palynology, v. 71, p. 17–35, doi:10.1016/0034-6667(92)90156-B.

Robaszynski, F., et. al, 1982, Le Turonien de la région-type: Saumurois et Touraine—Stratigraphie, biozonations, sédimentologie: Bulletin des Centres de Recherches Exploration-Production Elf–Aquitaine, v. 6, p. 119–225.

Røgen, B., I. L. Fabricius, P. Japsen, C. Høier, G. Mavko, and J. M. Pedersen, 2005, Ultrasonic velocities of North Sea chalk samples: Influence of porosity, fluid content and texture: Geophysical Prospecting, v. 53, p. 481–496.

Schober, A., and U. Exner, 2011, 3-D structural modelling of an outcrop-scale fold train using photogrammetry and GPS mapping: Austrian Journal of Earth Sciences, v. 104, p. 73–79.

Smith W. H. F., and P. Wessel, 1990, Gridding with continuous curvature splines in tension: Geophysics, v. 55, p. 293–305, doi:10.1190/1.1442837.

Steiner, B., E. H. Saenger, and S. M. Schmalholz, 2011, Timereverse imaging with limited S-wave velocity model information: Geophysics, v. 76, p. MA33–MA40, doi:10.1190/geo2010-0303.1.

Telford, W. M., L. P. Geldart, and R. E. Sheriff, 1990, Applied geophysics, 2nd Edition: Cambridge, Cambridge University Press, 792 p., ISBN 0-521-33938-3.

Urmos J., R. H. Wilkens, F. Bassinot, M. Lyle, J. C. Marsters, L. A. Mayer, and D. C. Mosher, 1993, Laboratory and well-log velocity and density measurements from the Ontong Java Plateau: New in-situ corrections to laboratory data for pelagic carbonates, in W. H. Berger, L. W. Kroenke, L. A. Mayer, et al., Proceedings of the Ocean Drilling Program Scientific Results 130, p. 607–622.